Role of loading direction on cyclic behaviour characteristics of AM30 extrusion and its fatigue damage modelling

Ali A. Roostaei, Hamid Jahed

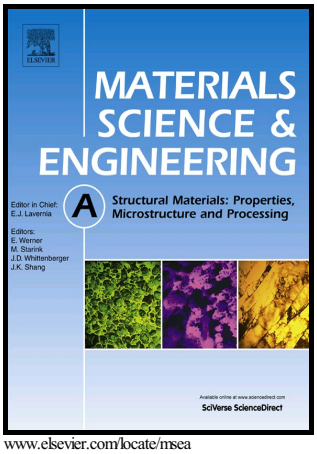

www.elsevier.com/locate/msea

PII: S0921-5093(16)30644-X
DOI: http://dx.doi.org/10.1016/j.msea.2016.05.116
Reference: MSA33744

To appear in: *Materials Science & Engineering A*

Received date: 7 May 2016
Revised date: 26 May 2016
Accepted date: 30 May 2016

Cite this article as: Ali A. Roostaei and Hamid Jahed, Role of loading direction on cyclic behaviour characteristics of AM30 extrusion and its fatigue damage modelling, *Materials Science & Engineering A* http://dx.doi.org/10.1016/j.msea.2016.05.116

Role of loading direction on cyclic behaviour characteristics of AM30 extrusion and its fatigue damage modelling

Ali A. Roostaei, Hamid Jahed *

Mechanical and Mechatronics Engineering Department, University of Waterloo, 200 University Ave. W. Waterloo, ON, Canada N2L 3G1

Abstract

Anisotropic fatigue and cyclic behaviour of AM30 Mg alloy extrusion is investigated by performing fully-reversed strain-controlled tension-compression cyclic tests at strain amplitudes between 0.3% and 2.3%, along extrusion (ED) and transverse (TD) directions. The shapes of half-life hysteresis loops suggest the predominance of slip and twinning/de-twinning mechanisms below and above the strain amplitude of 0.5%, respectively. The twinning/de-twinning occurrence is found to be more extensive during straining along ED, which results in higher asymmetry of hysteresis loops, and thereby, higher induced mean stress. This adversely affects the fatigue resistance and yields to less number of cycles before failure in ED. Optical microscopy and texture analysis are employed to validate the findings. In addition, fracture surfaces are studied by scanning electron microscopy to identify the sources of fatigue crack initiation. Persistent slip bands (PSBs) and twin lamellae interfaces are evidenced as crack initiation sites at low and high strain amplitudes, respectively. Cracks emanated from debonded inclusion interface are also observed. Lastly, estimated fatigue life by Smith-Watson-Topper (SWT) and Jahed-Varvani (JV) fatigue models are compared with experimental life obtained through this study as well as the ones reported in the literature. The JV energy model is proven to yield better life predictions.

Keywords: Magnesium alloys; Fatigue; Anisotropy; Texture; Twinning; Electron microscopy.

* Corresponding author.
Email addresses: aaroostaei@uwaterloo.ca (A.A. Roostaei), hjahed@uwaterloo.ca (H. Jahed).

1. Introduction

In recent years, the automotive industries' commitment to reduce vehicle's weight, and thereby fuel consumption, has brought more attention to light metals. Other than saving energy, weight reduction reduces greenhouse gas emissions, which, in turn, contributes to the conservation of environment [1]. Magnesium (and its alloys), being the lightest commercially available structural metal (with the density of 1.75 gr/cm^3), has undoubtedly been the focal point for this increased interest [2–6].

Currently, magnesium alloys are widely being applied to automotive components used in vehicle interior, housings and trim parts [7]. Extending current application of magnesium alloys to load-bearing components such as suspension arms requires, on one hand, comprehensive understanding of their plastic behaviour. On the other hand, fatigue modelling is necessary to estimate these components' service life under cyclic loading conditions.

Die casting has been the main manufacturing process for magnesium components [8,9]. Compared to cast products, wrought magnesium alloys have shown enhanced mechanical properties, e.g., tensile and fatigue properties [10–13]. However, the development of preferred orientation (texture) upon conventional forming/processing applications such as rolling and extrusion, renders their cyclic plastic and fatigue behaviour dependant on the loading direction. In this context, a number of previous researches have been dedicated to the anisotropic fatigue characteristics of wrought magnesium alloys along different directions [13–20].

Sajuri et al. [13] carried out stress-controlled cyclic tests on AZ61 extrusion along extrusion (ED), transverse (TD) and 45° to the ED and reported a higher fatigue strength in the ED compared to those in other directions. Lv et al. [16,17] investigated the strain-controlled cyclic response of rolled AZ31 alloy in rolling (RD) and transverse directions. They observed

that under the same total strain amplitude, the cyclic stress amplitudes of TD specimens were higher than those of RD specimens, while fatigue lives under both stress- and strain-controlled cyclic loadings were longer for TD. They, further, showed that strain-life data along both directions could be described by separate Coffin-Manson relations, but did not attempt to model consolidated fatigue damage data. In another study by Park et al. [15], rolled AZ31 Mg alloy plate was subjected to strain-controlled cyclic tests along RD and ND (normal to the plate). The ND was seen to exhibit superior fatigue resistance, which was ascribed to the beneficial compressive mean stress during cyclic deformation along ND. It was also concluded that total strain energy density (defined as the addition of positive elastic and plastic strain energy densities) as damage parameter was capable of correlating consolidated fatigue damage data considering directional anisotropy. A more recent work by Park et al. [14] on the same rolled AZ31 alloy plate under stress-controlled cyclic testing reported shorter fatigue life for ND specimens in comparison with RD specimens. They attributed this to the greater extent of plastic strain accommodation by twinning due to lower twinning stress while loading along ND. Lin et al. [21,22] explored the influence of sampling direction on the low-cycle fatigue life of hot rolled AZ91 alloy under stress-controlled cyclic tests with various stress ratios and peak stresses. Their results indicated that the fatigue lives of TD specimens were longer than those of RD specimens under all test conditions. Furthermore, they successfully used a modified Basquin model with two separate sets of parameters extracted from RD and TD data to estimate the experimental life. Finally, it was reported by Jordon et al. [18] that even though AZ61 extrusion, under the influence of texture, exhibited a slightly greater high-cycle fatigue resistance along ED compared to ND, inclusion size was the decisive parameter in obtained experimental fatigue life. They stated that fatigue behaviour differences along ED and ND could be captured by incorporating

the differences in grain orientation and size, particle size and cyclic hardening parameters into a multistage fatigue (MSF) model.

Wrought AM30 magnesium alloy is a Mg-Al-Mn alloy system developed by Luo and Sachdev in 2007 [23]. Henceforth, very limited number of studies [11,24–27] have been conducted on its cyclic and fatigue behaviour. Begum et al. [11] and Luo et al. [24] performed strain-controlled cyclic tests on an extrusion piece along ED at strain amplitudes between 0.1% and 0.6% and observed cyclic hardening and asymmetric hysteresis loops at high strain amplitudes. It was stated by the former study that Coffin-Manson and Basquin rules could be used to describe fatigue life. The effect of crystallographic orientation on fatigue of AM30 alloy crash rail extrusion was explored by Jordon et al. [25] through strain-controlled cyclic tests with amplitudes between 0.2% and 0.5%. Based on their results, the stress amplitude as well as mean stress for ED specimens (with most of basal planes parallel to loading direction) were higher than those in ND (with most of basal planes perpendicular to loading direction), and the ND specimens exhibited slightly better fatigue properties compared to ED ones. Moreover, in a parallel paper on AM30 extrusion under the same conditions, Lugo et al. [28] employed MSF model, with parameters calibrated separately for ED and ND, to fit experimental strain-life curves.

In spite of abovementioned literature on cyclic and fatigue characteristics of AM30 alloy, there is still lack of knowledge on its low-cycle fatigue response at high strain amplitudes up to 2.3%. More importantly, to the best of authors' knowledge, the in-plane (processing plane parallel to the basal planes of majority of crystals) fatigue and cyclic anisotropy, corresponding to different behaviour in ED and TD, has never been researched before. Fatigue damage modelling that incorporates material orientation is also lacking. The intent of present

investigation is, therefore, to look comprehensively into the orientation-dependent cyclic flow and fatigue behaviour of AM30 alloy extrusion along ED and TD, as well as cyclic damage analysis and fatigue life modelling.

2. Materials and Methods

2.1. Material and specimen

The material selected for current investigation is AM30 magnesium alloy processed by hot extrusion as detailed in [23]. The flat specimens for monotonic and cyclic tests with the geometry sketched in Figure 1, were machined from the extrusion section along two orthogonal directions i.e., extrusion (ED) and transverse (TD), corresponding to regions 'A' and 'B' in Figure 2, respectively.

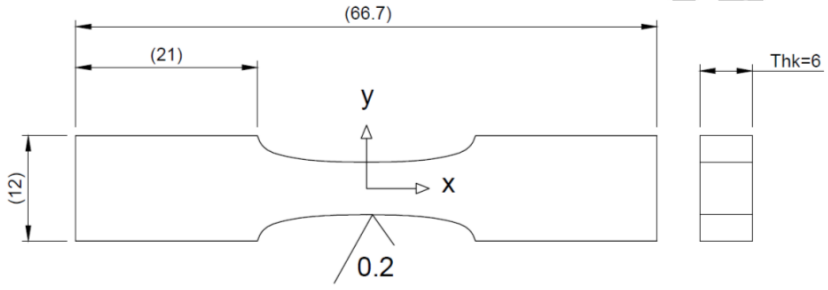

x (mm)	y (mm)	x (mm)	y (mm)
0.00	3.00	8.38	3.49
0.68	3.00	9.14	3.63
1.37	3.01	9.93	3.82
2.05	3.01	10.69	4.05
2.74	3.03	11.36	4.37
3.42	3.04	11.77	4.71
4.11	3.07	12.01	4.98
4.80	3.11	12.25	5.34
5.50	3.15	12.52	6.00
6.20	3.20	33.35	6.00
6.91	3.28	33.35	0.00
7.64	3.37		

Notes

1. All dimensions are in (mm) except the surface roughness which is in micro-meter.
2. Curvature of the reduced section is determined by the coordinates shown in the table.
3. Axes x and y are axes of symmetry.

Figure 1 Specimen geometry for tensile and fatigue tests.

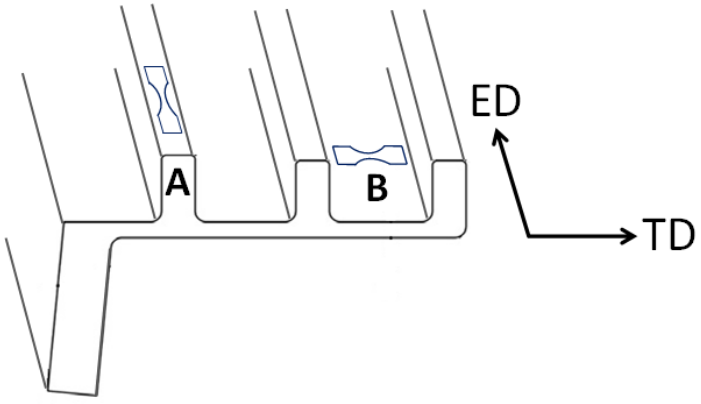

Figure 2 Schematic view of AM30 extrusion profile with locations of ED and TD specimens specified with letters 'A' and 'B', respectively.

Prior to microstructure observation via optical microscope, metallographic samples were manually ground using SiC papers and then sequentially polished with 6, 3, 1 and 0.1 μm diamond pastes. For the purpose of revealing grain (twin) boundaries in the microstructure, acetic-picral etchant solution (4.2 g picric acid, 10 mL acetic acid, 10 mL distilled water, 70 mL ethanol) was used. A typical initial microstructure of the experimental AM30 alloy is shown in Figure 3. According to this figure, twin-free grains with bimodal size distribution are observed. A similar microstructure for AM30 extrusion was reported along ED and TD [24]. It was also reported that the top and bottom surfaces of the extrusion section consisted of larger grains than that of center region [11]. This has been heeded, for comparative purposes, while machining the specimens.

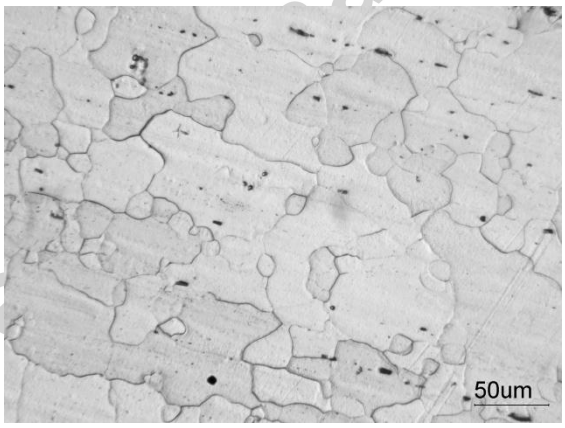

Figure 3 Initial twin-free microstructure of experimental AM30 alloy.

Texture measurements were carried out on a Bruker D8 Discover X-ray diffractometer equipped with a VÅNTEC-500 2D detector using Cu-K_α beam radiation at 40 kV and 40 mA. The use of area detector enabled automated defocusing and background corrections of peak profile. The initial textures of regions 'A' and 'B' of the extrusion section represented by pole figures of basal (0002) and prismatic $(10\bar{1}0)$ poles are displayed in Figure 4(a) and (b),

respectively. Both regions evince strong basal textures, with the majority of crystals having their c-axes tilted about 20° from ND toward ED in Figure 4(a) and nearly perpendicular to ED in Figure 4(b).

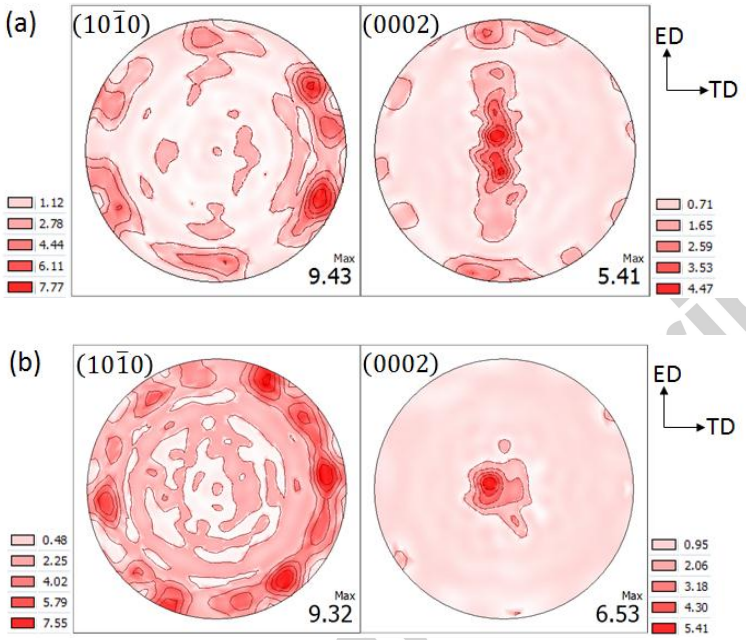

Figure 4 (0002) and (10$\bar{1}$0) pole figures of AM30 extrusion at locations (a) 'A', and (b) 'B'.

2.2. Fatigue testing setup

Fatigue testing was performed on an Instron 8874 servo-hydraulic load frame with 25 kN axial force capacity. Fully reversed ($R_\varepsilon = -1$) strain-controlled tension-compression (pull-push) cyclic tests, as per ASTM standard E606, were conducted at ambient temperature. The tests were run at varying frequencies between 0.02 and 0.2 Hz depending on the applied strain amplitude. Engineering strain values were recorded and controlled through a uniaxial extensometer with gauge length of 10 mm and travel of ±0.8 mm. At very low strain amplitudes, after material stabilized, i.e., when the maximum and minimum loads of each cycle stayed unchanged from one cycle to the next, tests were switched to load-controlled cycling at higher frequencies up to 15 Hz. Test stopping criteria were considered either final rupture of the specimen or 50% load drop.

Afterwards, the final fracture surfaces were inspected for crack initiation and propagation mechanisms employing scanning electron microscope (SEM) in secondary electron (SE) mode.

3. Results

3.1. Monotonic tensile behaviour

The monotonic uniaxial stress-strain response of the AM30 extrusion along ED and TD are given in Figure 5(a). The initial portions of the curves (up to the axial strain of 0.05), which is of more importance to the argument being made by this study, are redrawn in Figure 5(b). A noticeable yielding anisotropy is present between ED and TD. Yield stress (0.2% offset) along ED is measured to be roughly twice that along TD (200 MPa as against 117 MPa). Since loading orientation is not preferable for twinning activation, the yielding anisotropy hints at the activation of different slip systems during tension along ED and TD. Employing crystal plasticity simulations to calculate Schmid factor for various slip systems during tensile deformation of magnesium alloys with similar texture as the one under investigation, it was concluded by other researchers [25,29] that basal slip $\{0001\}\langle 11\bar{2}0\rangle$ and prismatic slip $\{10\bar{1}0\}\langle 11\bar{2}0\rangle$ are predominant slip mechanisms for accommodating tensile strain along TD and ED, respectively. This seems to contradict the very high critical resolved shear stress (CRSS) for prismatic slip at room temperature. It was, however, reported that aluminum as alloying element in Mg-Al alloys facilitated room-temperature slip on prismatic planes at the same time with strengthening of basal planes against slip [30–33]. Higher CRSS for slip on prismatic planes at room temperature is then expected to reflect the observed yielding behaviour.

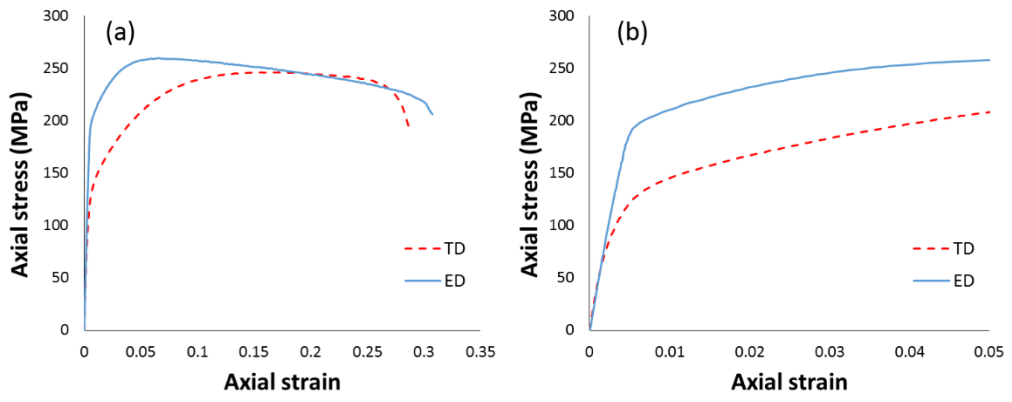

Figure 5 (a) Tensile stress-strain curves of AM30 extrusion with loading direction along ED and TD, (b) Zoomed-in details up to 5% strain.

3.2. Fully reversed strain-controlled cyclic test results

3.2.1. Extrusion Direction (ED)

Figure 6 shows the half-life stress-strain hysteresis loops of AM30 Mg alloy extrusion specimens cut along ED under fully reversed strain-controlled pull-push tests at different strain amplitudes ranging from 0.3% to 2.3%. The shapes of half-life hysteresis loops at various strain amplitudes are mainly dictated by the occurrence and exhaustion of twinning and de-twinning as governing plastic deformation mechanisms. At low strain amplitudes of 0.3% and 0.4%, very little plastic deformation can be detected. Judging by the absence of macroscopic flow manifestation of twins, the plastic deformation should principally be accommodated by basal and non-basal slip systems [34,35] with predominance of prismatic slip as was stated before. This means that the compressive stress of -118 MPa under the strain amplitude of 0.4% is obviously not enough to get the twins dominantly activated at the half-life. However, the strain amplitude of 0.5% provides sufficient stress (-124 MPa) to trigger extension twinning $\{10\bar{1}2\}\langle 10\bar{1}1\rangle$ and de-twinning in the compressive and tensile reversals, respectively. Henceforth, marked flow asymmetry under tension and compression is observed. De-twinning during tensile reversals (for $\varepsilon_a \geq 0.5\%$) happens readily inside the twinned portion of grain and results in a decreased

hardening rate [36–38]. Upon de-twinning exhaustion, slip takes over and the hardening rate is subsequently increased, causing an inflection point in the tensile reversal. The increased hardening rate is known to be due to the rotation of crystals to hard orientations for higher order slip and the activation of compression twinning $\{10\bar{1}1\}\langle 10\bar{1}2\rangle$ [32,39–42]. The same inflection point in the compressive reversal, attributed to the saturation of twinning, is observed for strain amplitudes greater or equal to 1.5%. Similarly to the tensile reversal, slip plays the major role upon saturation of twinning as deformation mechanism. Impeding dislocation movements by twin boundaries, then, contributes to the higher hardening rate of the flow curve. This results in attenuated flow asymmetry between tension and compression at high strain amplitudes, as is seen from Figure 8(c).

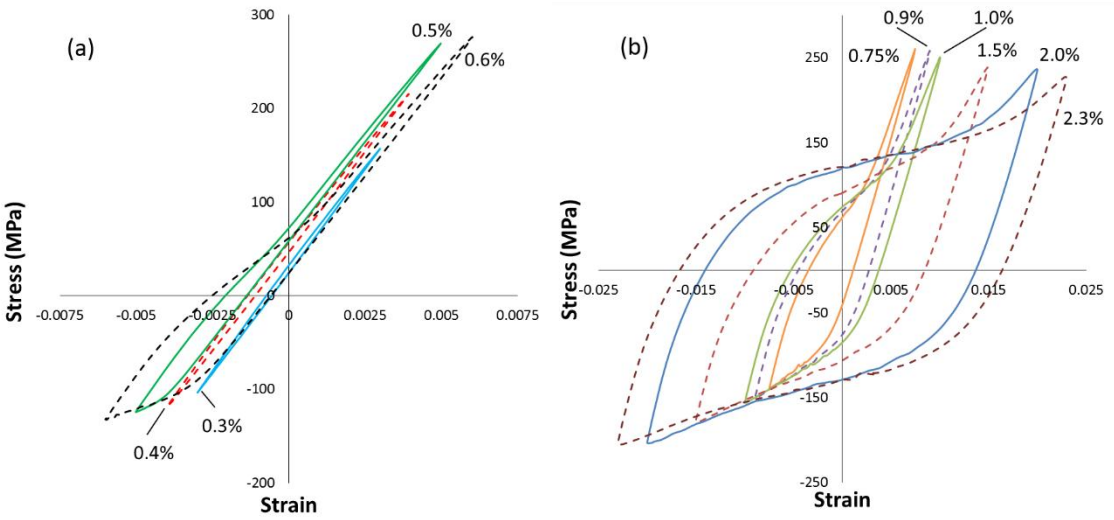

Figure 6 Half-life hysteresis loops of AM30 extrusion tested at various strain amplitudes along ED.

The variations of stress amplitude and mean stress for specimens along ED during strain-controlled pull-push tests are plotted in Figure 7. Generally, AM30 alloy extrusion hardens under cyclic straining along ED [11,25]. This may be related to the formation of residual twins during successive processes of twinning and de-twinning in each cycle [36]. To be more specific, the hardening response changes with strain amplitude. Accordingly, three distinct types of hardening

behaviour can be inferred from Figure 7(a). Firstly, at strain amplitudes of 0.3% and 0.4%, stress amplitude is constant during the initial 10 cycles, then the material slightly hardens before reaching to stability again. As is shown in Figure 8(a), at 0.3%, deformation starts with twinning during compression and de-twinning in tensile reversal. This leads to the formation and build-up of residual twins after each cycle, which brings about the cyclic hardening. When twinning gets deactivated, the residual twin build-up and hardening cease. Secondly, at strain amplitudes between 0.5% and 1%, an increasing trend for stress amplitude is observed with progression of straining. Finally, strain amplitudes greater or equal to 1.5% (Figure 8(c)) will cause the material to harden at first, and then become stable until failure. This points out that the capacity of microstructure for residual twins is saturated [36].

Mean stress variations with cyclic deformation corresponding to the mentioned three ranges are: no change or gradual increase for low strain range, rapid increase or no change for medium strain range, and rapid decrease for high strain range (Figure 7(b)). The increasing trend for mean stress with cycling can be corresponded to the increase in peak stress in tensile reversal. This phenomenon has been argued to be due to the transformation of mobile dislocations in parent matrix to immobile ones in the substructure of $\{10\bar{1}2\}\langle 10\bar{1}1\rangle$ tension twins upon 86.3° lattice rotation [43,44]. The rationale behind the observed decaying of mean stress with cyclic test progression at high strain amplitudes will be discussed later.

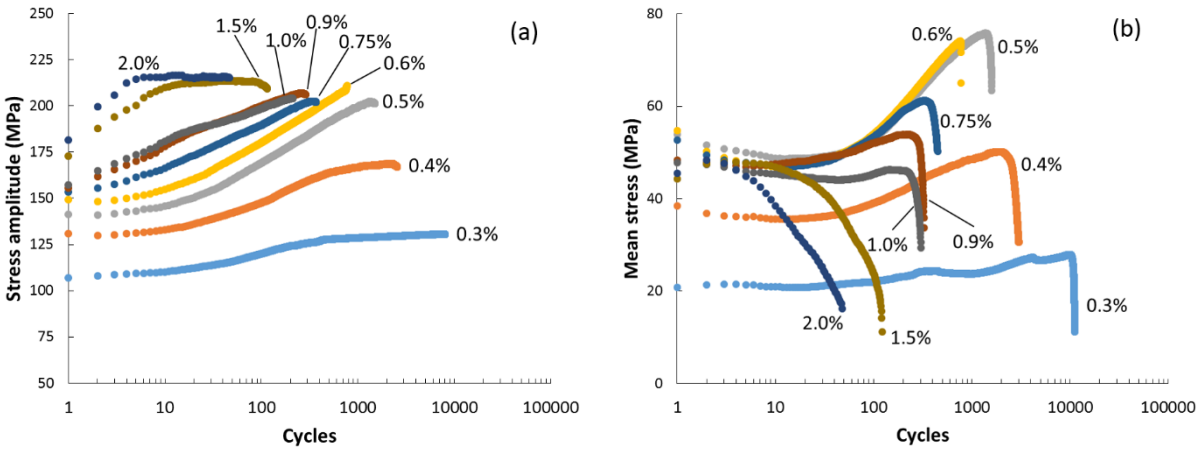

Figure 7 Variations of (a) stress amplitude and (b) mean stress with number of tension-compression cycles at various strain amplitudes along ED.

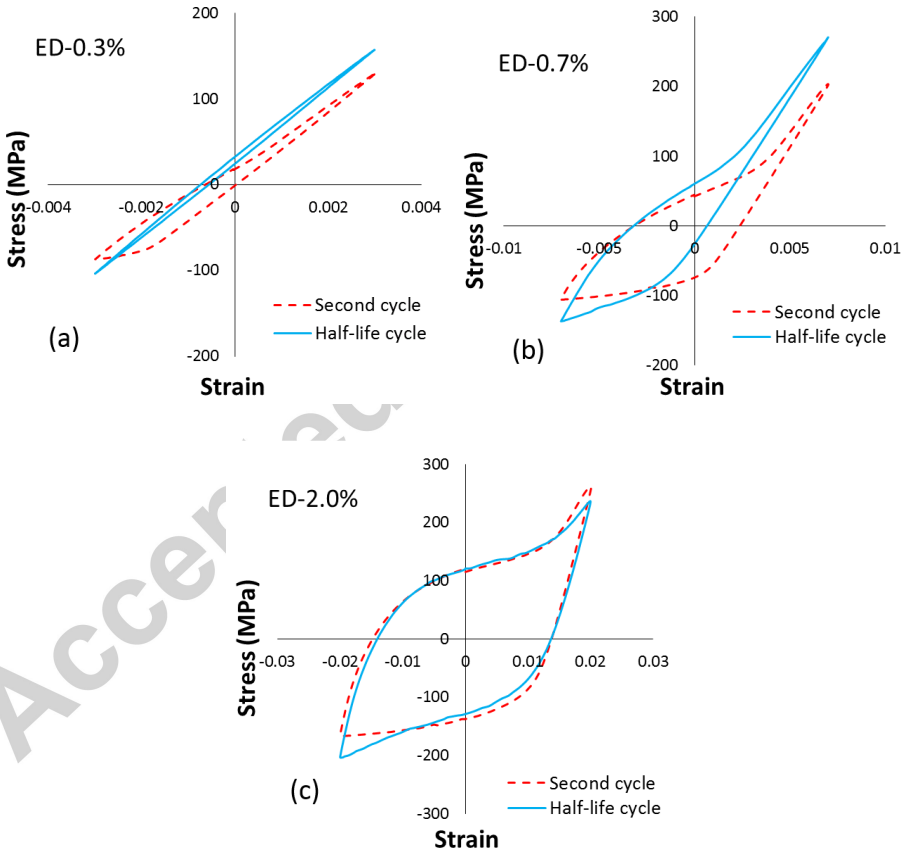

Figure 8 Typical hysteresis loops of ED specimens at second and half-life cycles during cyclic tests at (a) low, (b) intermediate, and (c) high strain amplitudes.

3.2.2. Transverse Direction (TD)

The half-life stress-strain hysteresis loops of AM30 Mg alloy extrusion specimens tested under the same conditions as Figure 6 but along TD, are illustrated in Figure 9. According to Figure 9(a), twinning becomes the predominant plastic deformation mode at strain amplitudes equal to or greater than 0.5% corresponding to the compressive stress of -118 MPa. This stress level was seen to be insufficient for twinning activation in ED. Since CRSS for twinning is much higher than that for basal slip, TD specimens, which are more favourably oriented for basal slip, exhibit lower stress levels during compression [29]. From another point of view, the lower compressive stress in TD can be, indirectly, connected with the lower extent of twin formation.

Below 0.5%, hysteresis loops exhibit considerable plastic strain being primarily accommodated by basal slip. Moreover, twinning exhaustion, which is depicted by the inflection point in the compressive reversal, is observed for strain amplitudes higher than 1.2%.

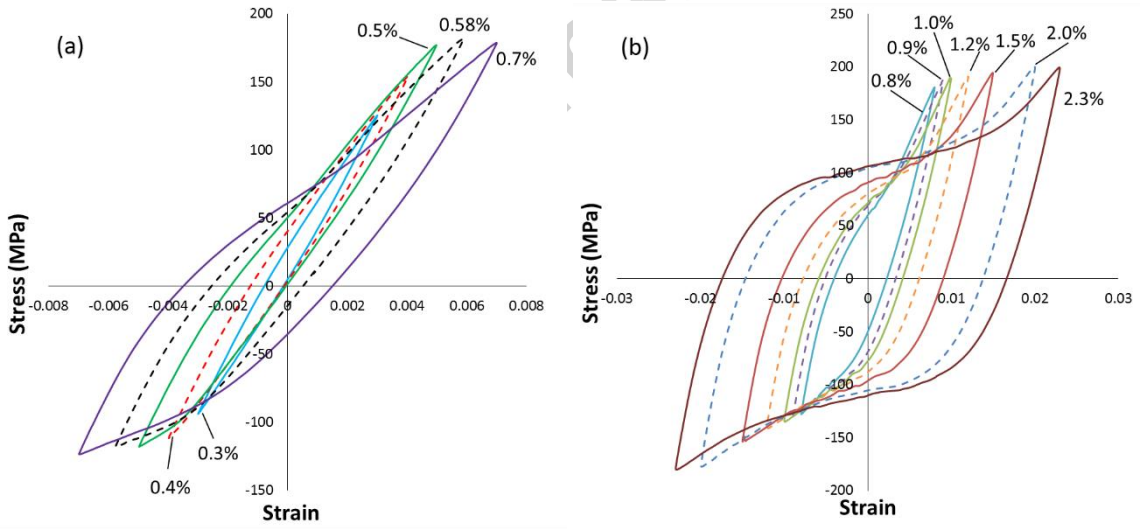

Figure 9 Half-life hysteresis loops of AM30 extrusion tested at various strain amplitudes along TD.

Plots of stress amplitude and mean stress variations against number of cycles illustrated in Figure 10, confirm the overall hardening of AM30 extrusion along TD. As in ED, three types of hardening behaviour can be identified. The strain amplitudes of 0.3% (Figure 11(a)) and 0.4% are characterised with no hardening associated with mean stress decay during initial 10-20 cycles

followed by gradual increase in both hardening rate and mean stress. Similar to behaviour in ED, residual twins' formation are believed to be the reason. Between 0.5% and 1.5%, cyclic hardening occurs throughout the whole life with increasing or steady mean stress. Typical second and half-life cycles related to this type of behaviour is shown in Figure 11(b). At high strain amplitudes of 2% (Figure 11(c)) and 2.3%, the hardening essentially ceases after 10 cycles as a result of residual twin saturation. It is noteworthy that hardening saturation happens at a larger strain amplitude along TD than ED. This delayed saturation is consistent with the less favourability of twinning in compression along TD. For these high strain amplitudes, mean stress evolution shows a sustained decrease up until failure, which will be discussed hereunder.

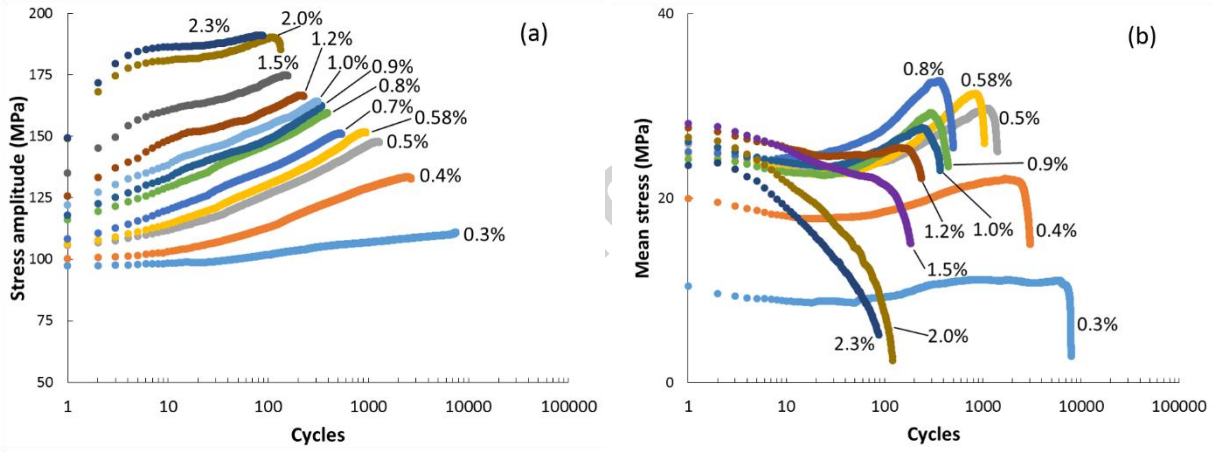

Figure 10 Variations of (a) stress amplitude and (b) mean stress with number of tension-compresssion cycles at various strain amplitudes along TD.

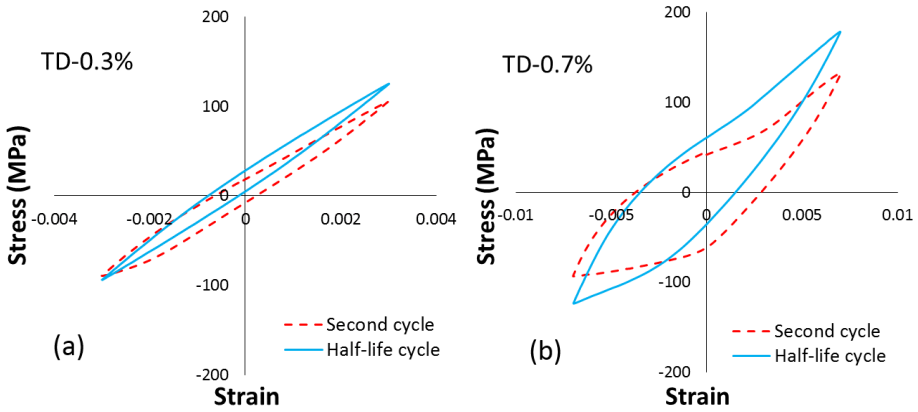

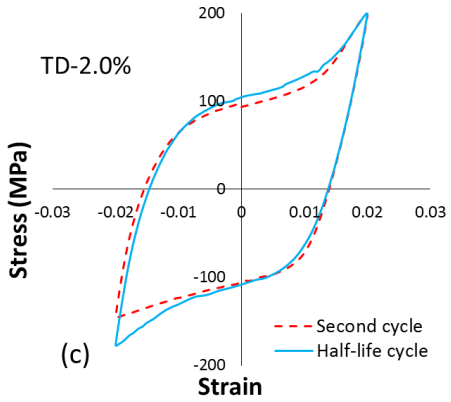

Figure 11 Typical hysteresis loops of TD specimens at second and half-life cycles during cyclic tests at (a) low, (b) intermediate, and (c) high strain amplitudes.

3.3. Microstructure and texture analyses

Typical optical micrographs of AM30 Mg alloy extrusion tested under low and high strain amplitudes are presented in Figure 12. Figure 12(a) and (b) show the microstructures of ED specimens tested at strain amplitudes of 0.3%.and 2%, respectively. Twin-free grains in the microstructure of specimen subjected to low strain amplitude of 0.3% (Figure 12(a)) confirms the predominance of slip mechanism mentioned before in the context of hysteresis shapes. However, some traces of residual twins can be evidenced inside the microstructure (yellow arrows), which is in line with the stress amplitude evolution with cycling at low strain amplitudes described earlier. The irregular stepped appearance of these twins is most likely due to the interaction of twinning dislocations on twin boundary and defects such as dislocation pile-ups in matrix during slip-driven deformation [44,45]. Contrary to low strain amplitude, microstructure at high strain amplitude (Figure 12(b)) displays extensive twinning (mainly c-axis tension twins $\{10\bar{1}2\}\langle 10\bar{1}1\rangle$ judging by their lenticular morphology [24,46]) inside almost all grains. As is seen, the twins consume their parent grains and in some grains twins in different orientations intersect each other. Besides, twins without visible boundaries, shown by arrows in Figure 12(b), indicate the occurrence of twin growth and coalescence, as discussed in [47,48].

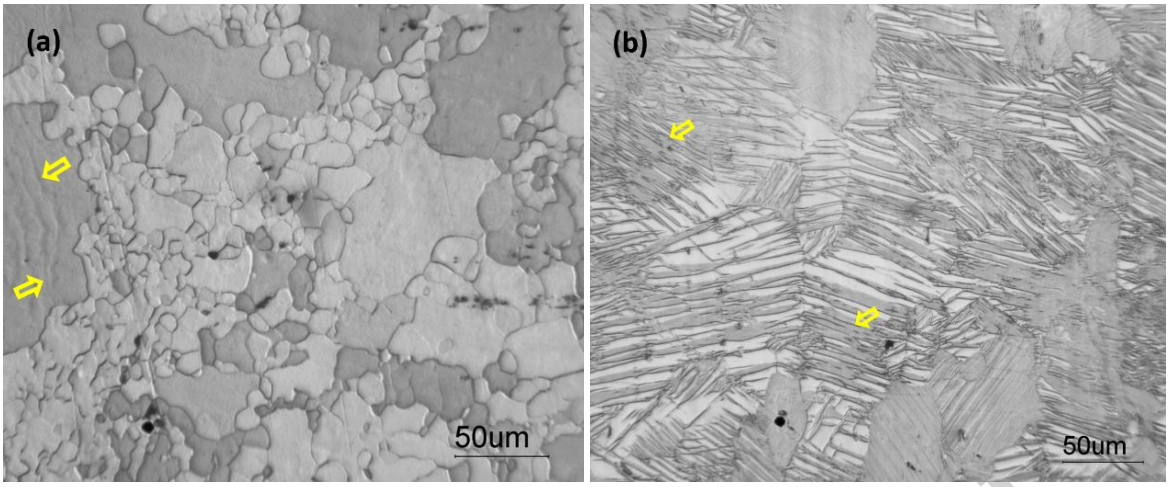

Figure 12 Optical microstructures after cyclic pull-push tests along ED at (a) 0.3%, and (b) 2%.

Figure 13 shows texture measurements represented by pole figures of basal (0002) and $(10\bar{1}0)$ prismatic poles for specimens tested at various strain amplitudes and along different directions: (a) 0.3% in ED, (b) 2% in ED, (c) 0.3% in TD and (d) 2% in TD. The XRD measurements were done on sections far away from the final fracture surface. It should also be mentioned that all the specimens used for texture analysis had been fractured under tension. Comparing pole figures in Figure 13(a) and (c) with as-extruded ones (Figure 4) reveals that, in general, the main texture components are preserved after cyclic straining at 0.3%, which is in accordance with slip being the predominant deformation mode as was previously assumed. Furthermore, it is seen that some of the basal poles are oriented from nearly normal/normal direction (ND) towards ED. This change in orientation cannot be related to slip. It can, however, be justified by twinning, which causes the basal planes to rotate 86.3°. The observation of residual twins in the microstructure shown in Figure 12(a) corroborates the mentioned justification.

On the other hand, texture of the specimens subjected to the strain amplitude of 2% represented by pole figures in Figure 13(b) and (d), indicates a drastic change in the texture, which can be ascribed to the occurrence of profuse extension twinning. This change is realized

by vanishing of most of the basal poles in the center (ND) of (0002) pole figures and formation of new components along TD and ED, for specimens tested in ED and TD, respectively. In other words, the c-axes of majority of grains are rotated away from the straining direction and oriented against compression [49]. This is the favourable orientation for the activation of bulk extension twinning during the next compressive reversal. Additionally, higher maximum intensity of basal poles in Figure 13(b) (10.62 multiples of uniform distribution, MUD) compared to Figure 13(d) (8.05 MUD) is indicative of higher extent of twinning/de-twinning during deformation along ED.

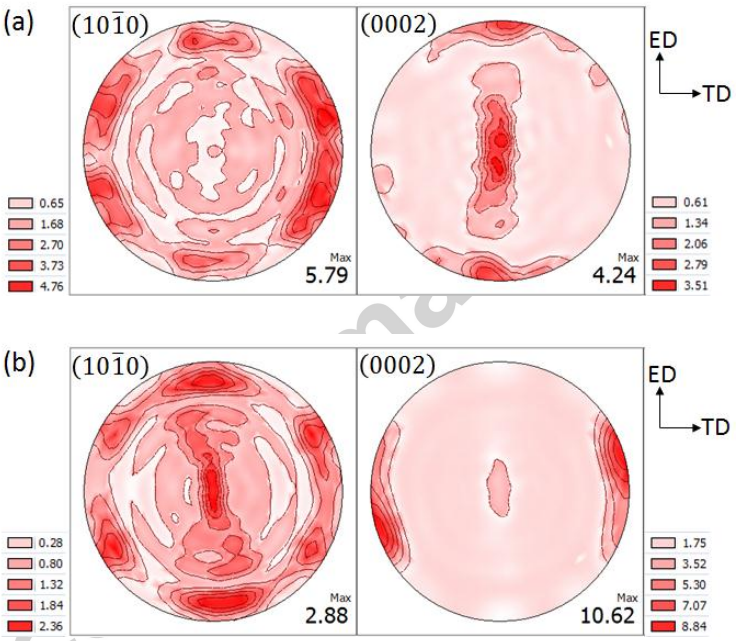

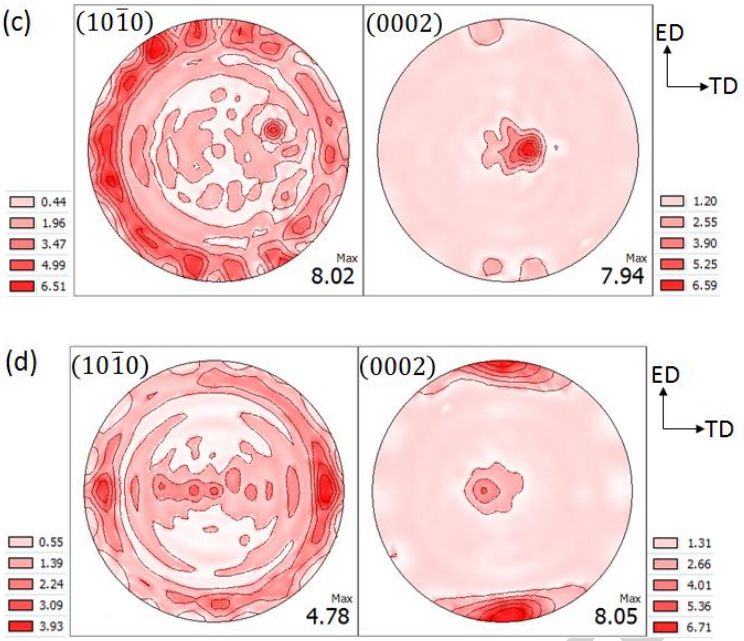

Figure 13 (0002) and $(10\bar{1}0)$ pole figures of AM30 extrusion specimens subjected to cyclic tests at: (a) 0.3% in ED, (b) 2% in ED, (c) 0.3% in TD, and (d) 2% in TD.

3.4. Fracture surface characterisation

The typical SEM images of the fracture surface for ED specimen tested at low strain amplitude of 0.3% is shown in Figure 14. Two distinct regions of crack initiation/stable propagation (region I) and unstable crack propagation (region II) are demarcated by a yellow line. These regions are identified with distinguishing features such as fatigue striations (Figure 14(c)) and river pattern for regions I and II, respectively [50]. Although a number of researchers [36,51,52] attributed the fatigue striations in magnesium alloys to sequential twinning/de-twinning processes, the observed striations in Figure 14(c) are probably due to slipping, bearing in mind the predominance of slip at low strain amplitudes. On closer observation of region I, multiple cracks are spotted emanating from the free surface. A magnified view of one of these crack initiation sites is depicted in Figure 14(b). It is clearly seen that the crack is originated at an extrusion-intrusion location at the surface (crack is designated with yellow arrow). These extrusion-intrusion features are results of persistent slip band (PSB) formation during slip-

controlled cyclic process. The PSBs, are, in turn, formed due to irreversible dislocation glide, i.e., when individual glide process is not perfectly reversed upon strain reversal [53,54]. Furthermore, the wavy appearance of slip lines is characteristic of the cross-slip of <a>-type dislocations into non-basal slip planes [55]. These findings are in agreement with macroscopic flow curves presented earlier, as well as crack initiation mechanisms reported for various magnesium alloys in the literature [56–60].

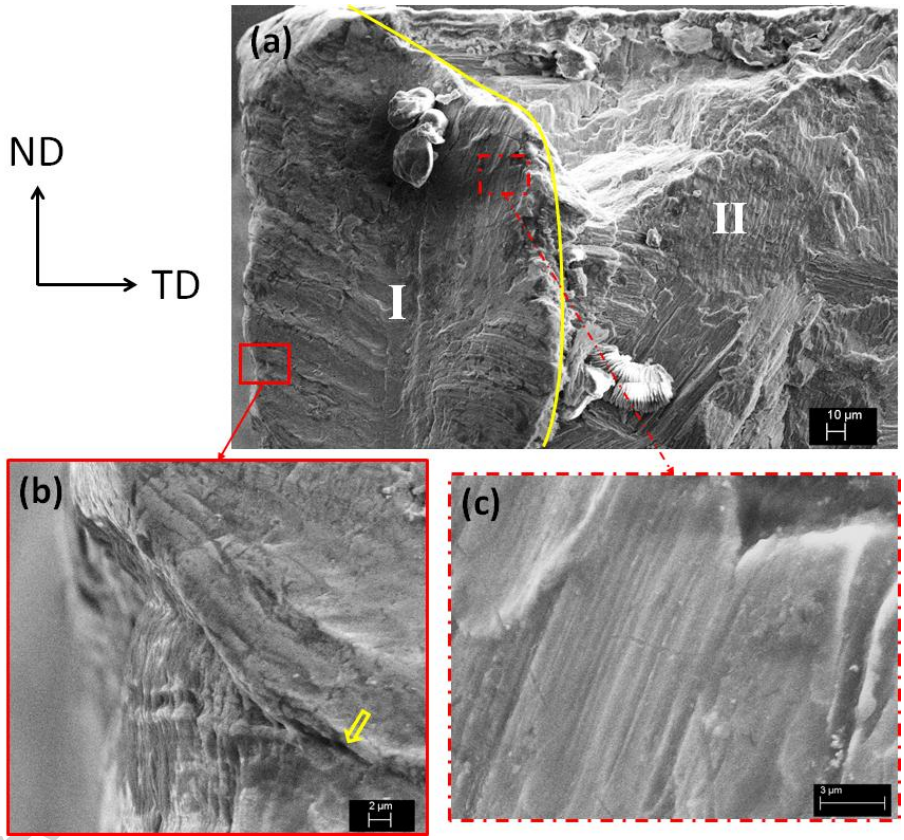

Figure 14 (a) SEM micrograph of AM30 typical fatigue fracture surface at low strain amplitude (0.3% in ED) showing regions I and II of crack propagation, as well as higher magnifications of (b) crack initiation site at surface with arrow pointing at the crack, and (c) fatigue striations corresponding to region I.

In addition to slip-band cracking, other crack initiation mechanisms are also observed for magnesium alloys, namely, twin-boundary cracking and inclusion cracking. For the magnesium alloy under investigation, cracks are evidenced to initiate at the twin lamellae interfaces at higher strain amplitudes. For instance, typical twin-boundary cracks (pointed by arrows in Figure 15)

are captured by SEM near the surface of the specimen tested at 1.5% along ED. At such high strain amplitudes no notable crack initiation site was observed, or rather simultaneous cracking sites at different locations were pinpointed [11,18,60,61]. Inclusions (intermetallic particles) are found to be the common crack initiators for AM30 magnesium alloy under various loading conditions along different directions. These inclusions were analyzed to be Al-Mn binary phases [25,62,63]. A crack can be induced by a fractured inclusion, or by debonding at inclusion-matrix interface. Only the cracked intermetallic particles in AM30 alloy were witnessed in previous works [25,62]. Nonetheless, an indication of a crack generated at debonded inclusion-matrix interface for TD specimen tested at 0.3% is shown in Figure 16. Yellow arrow points to the crack in the zoomed view of the inclusion-matrix interface.

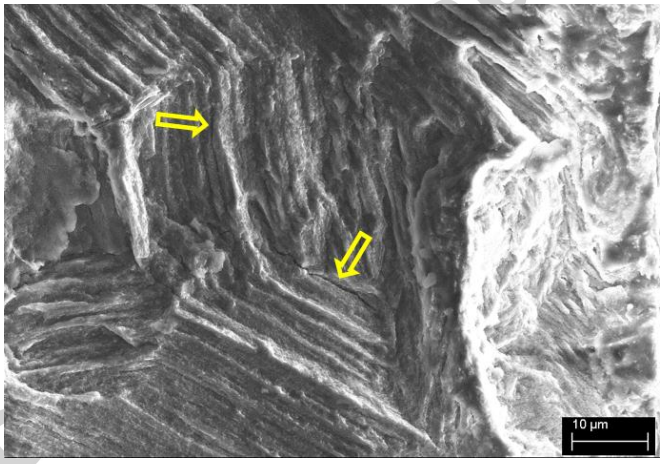

Figure 15 Twin lamellae as sources of fatigue cracks in AM30 at high strain amplitudes.

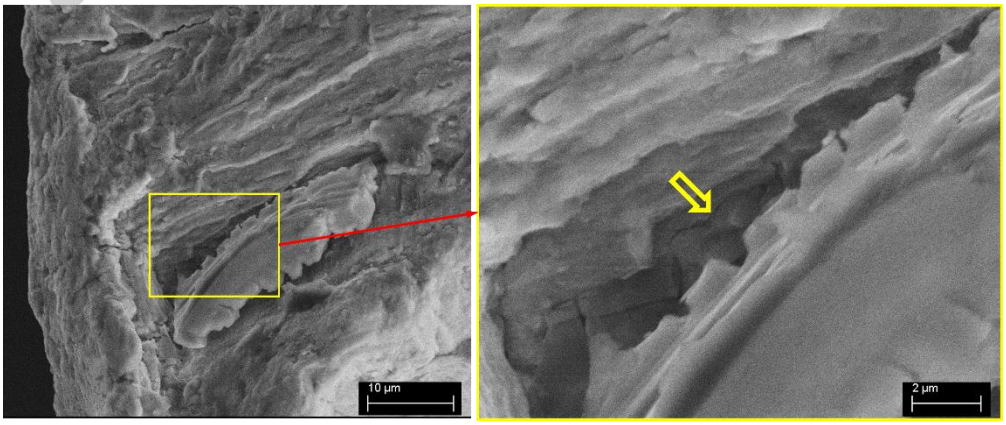

Figure 16 Typical SEM image of a fatigue crack originated from delaminated inclusion-matrix interface in TD specimen tested at 0.3%.

3.5. Strain-life curve

Total strain amplitude as a function of number of cycles to failure for specimens tested along ED and TD are presented in Figure 17(a). According to the results, ED specimens exhibit inferior fatigue properties compared to TD specimens over almost entire strain range tested in this investigation. The lower fatigue resistance demonstrated upon straining along ED may be explained by higher fatigue damage induced by means of more extensive twinning, as was deduced from flow characteristics in ED and TD. Mean stress effects should be also taken into account, which will be done so further on. The strain-life results are consistent with the previous studies on the direction-dependent fatigue behaviour of rolled AZ31 magnesium alloy [16,17].

For comparison purposes, strain-life results for AM30 extrusion tested in ED and ND at strain amplitudes up to 0.6%, taken from literature, are plotted in Figure 17(b), together with data from present study. It should be noted here that 0.6% is the maximum strain amplitude reported for cyclic testing of AM30 extrusion, hence, data up to 0.6% from present investigation are shown in Figure 17(b). The ED results are seen to be scattered, especially at strain amplitude of 0.3%. It is also noticed that ND demonstrates different fatigue properties at and below 0.5%. Their relatively lower fatigue life below 0.5% may be correlated with the fact that ND specimens are most favourably oriented for triggering extension twins during first tensile reversal [15,25]. At strain amplitude of 0.5%, however, the twins are found to be nucleating along all directions. Under this circumstance, ED specimens, with highest developed mean stress, show less number of cycles before failure.

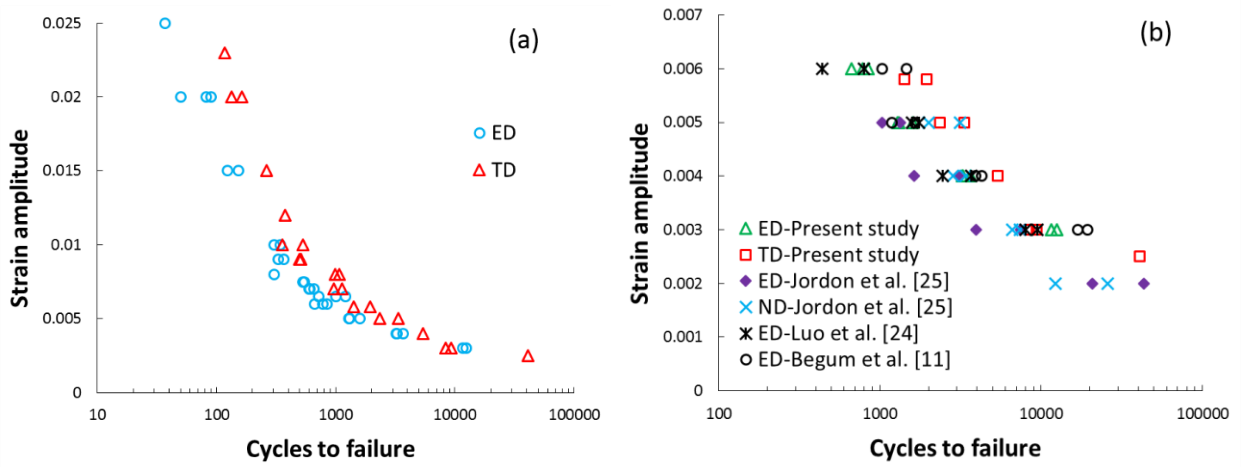

Figure 17 Strain-life data for AM30 extrusion along different directions: (a) obtained in the present study; (b) a comparison with results reported in literature.

4. Discussion

4.1. Cyclic stress-strain amplitude curves

In order to better understand the role of material anisotropy on the cyclic deformation behaviour of AM30 extrusion along two orthogonal directions, three undermentioned curves are extracted from half-life hysteresis loops and plotted against corresponding strain amplitude. Firstly, the plot of stress amplitude versus plastic strain amplitude for two directions is depicted in Figure 18(a). It is obvious that, to reach to the same amount of plastic deformation, higher levels of stress are needed when deforming along ED rather than TD. This is in tune with the more asymmetric hysteresis loops observed in ED (Figure 9), which can be related to higher volume fraction of twins activated during compressive reversal [29].

It is also to be noted that stress amplitude variation in TD exhibits an ascending trend, whereas in ED it shows minimal change after the strain corresponding to the activation of twinning. The reason lies probably in the way peak stress at the tip of tensile reversal in ED evolves, as is illustrated in Figure 18(b). This descending trend (softening) for the stress at tensile tip has been also reported for pure polycrystalline magnesium and ZK60 alloy extrusion

strained along ED, and was attributed to the ceaseless occurrence of grain boundary and twin tip cracking with the start of deformation [37,64]. From this perspective, the lesser extent of twinning while deforming along TD can explain the observed trend for the stress at the tensile tip of TD hysteresis loops with increasing strain amplitude.

Figure 18(c) illustrates the mean stress developed in different directions as a result of applied strain amplitude. It can be seen that for the same strain amplitude, the induced mean stress in ED specimens stays on top of TD results, which alludes to a higher fatigue damage inflicted during cyclic deformation along ED.

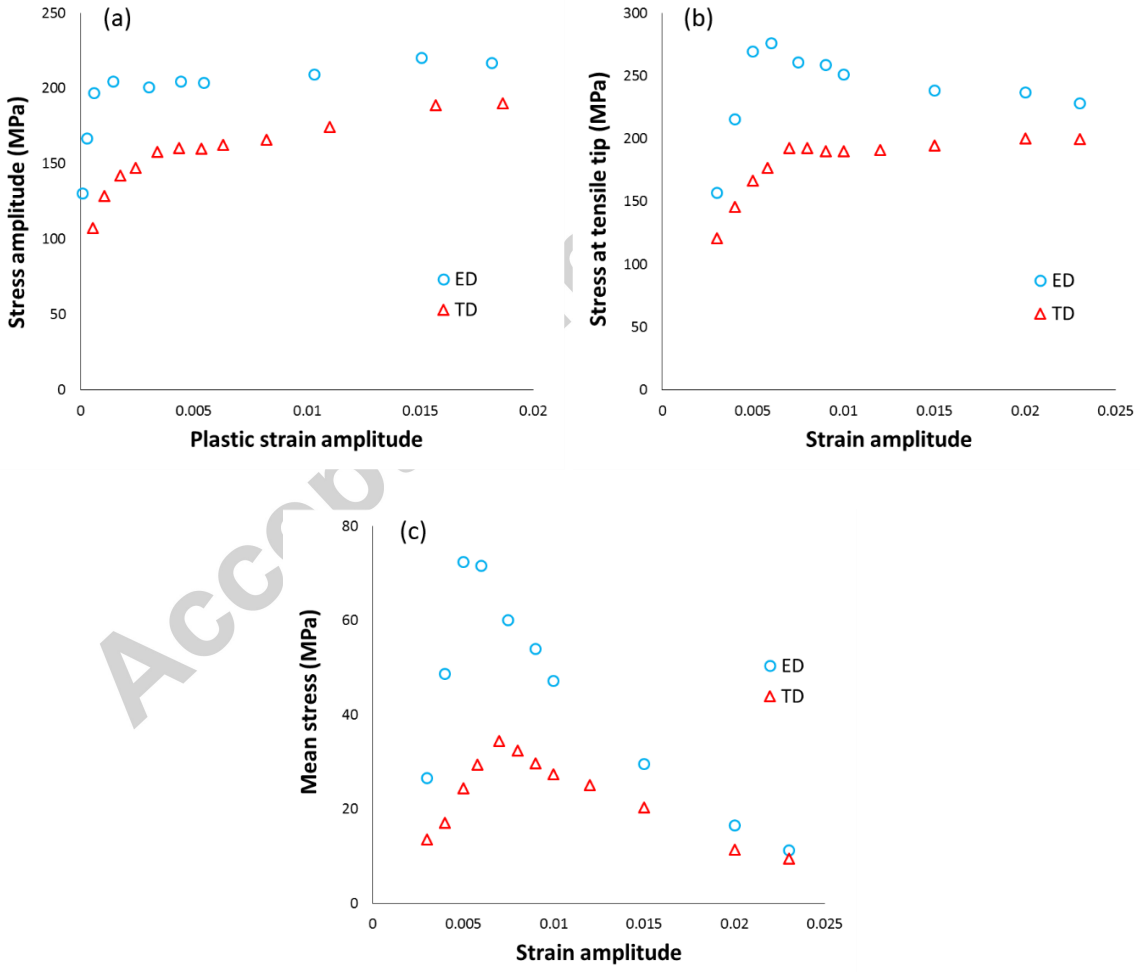

Figure 18 (a) Cyclic stress-plastic strain amplitude; variations of (b) stress at tensile tip and (c) mean stress with strain amplitude. Data extracted from half-life hysteresis loops in ED and TD.

4.2. Fatigue life modelling

In order to quantify the damage occurred in the microstructure of a material during cyclic loading, a number of fatigue damage parameters have been proposed and formulated in such a way that incorporates experimental fatigue life [65–67]. Available fatigue damage parameters can be categorized into stress-, strain- and energy-based methods. As was seen in Figure 18, for AM30 extrusion, a larger applied strain amplitude does not necessarily produce higher peak stress or mean stress, while, it definitely ends in less number of cycles before failure. Hence, a stress-based fatigue damage parameter cannot properly describe the inflicted fatigue damage in the Mg alloy under this investigation. However, stress-based fatigue life prediction models have been employed by Lin et al. [68] for AZ31B Mg alloy under stress-controlled loading. In what follows, a strain-based and an energy-based fatigue damage criteria are being evaluated based on their capabilities to predict the anisotropic fatigue data of AM30 extrusion.

4.2.1. Smith-Watson-Topper (SWT)

The SWT parameter, initially formulated for mean stress effect consideration, has been employed by many researchers for multiaxial fatigue analyses as a strain-based critical plane approach [69,70]. This parameter is written in terms of fatigue life:

$$\sigma_{n,max}\frac{\Delta\varepsilon_1}{2} = \frac{\sigma_f'^{\,2}}{E}\left(2N_f\right)^{2b} + \sigma_f'\varepsilon_f'\left(2N_f\right)^{b+c} \quad (1)$$

where $\Delta\varepsilon_1/2$ is the principal normal strain range, $\sigma_{n,max}$ is the maximum normal stress on maximum normal strain plane (as the critical plane) and E is the modulus of elasticity which was calculated, from the tensile tests, to be 43.8 GPa. The Coffin-Manson coefficients and exponents on the right-hand side of Eq. (1) are extracted from Figure 19(a) and listed in Table 1. The

symbols in Figure 19(a) corresponds to the experimental data obtained from half-life hysteresis loops along TD and the dashed lines represent the best power-law fits.

Table 1 Coffin-Manson parameters for SWT model.

Fatigue strength coefficient, σ_f' (MPa)	410.416
Fatigue toughness coefficient, ε_f'	1.480
Fatigue strength exponent, b	-0.130
Fatigue toughness exponent, c	-0.791

Figure 19(b) shows the SWT parameter calculated for each cyclic test condition as a function of number of reversals to failure. The data from literature are also included. From this plot, the relationship between SWT parameter and fatigue life in terms of reversal count can be fairly expressed using a single power-law relation. This implies that the SWT parameter can be utilized to quantify the fatigue damage imposed upon straining in different directions.

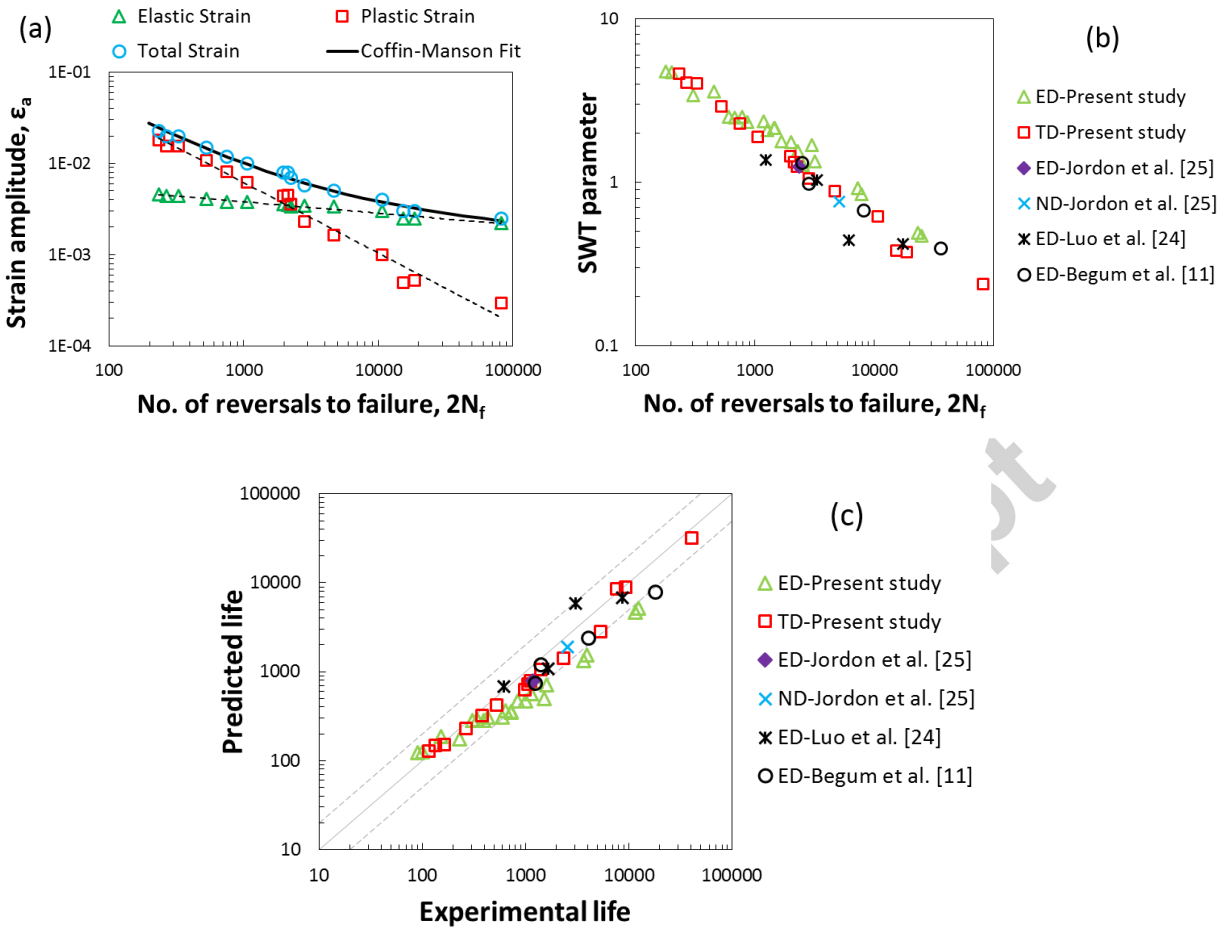

Figure 19 (a) Strain-life data used for extracting Coffin-Manson constants; (b) SWT damage parameter evolution with number of reversals to failure; (c) The correlation of SWT-estimated fatigue life with experimental life.

The predicted fatigue life, calculated from Eq. (1) in conjunction with values from Table 1, is plotted against the experimental life in Figure 19(c). The diagonal solid line denotes the perfect match and the other two dashed lines stand for factor of 2 bounds between predicted and experimental life. The life estimations are mostly found to be within a life factor range of 2, though for a few tests (mostly in ED) the lives are under-predicted. There is also some scatter seen in, especially, the ED predictions. These observations can be ascribed to the maximum normal stress parameter in SWT equation, Eq. (1), as its evolution with increasing strain amplitude was seen to be unusually complex (Figure 18(b)).

4.2.2. Jahed-Varvani (JV)

Energy-based fatigue damage model is another commonly used approach, especially for anisotropic materials. This is because of the invariant nature of strain energy density, being a scalar quantity. In this study, Jahed-Varvani energy model, which was introduced in 2006 [71], will be employed for fatigue life estimation. In the JV model, total energy density as damage parameter is assumed to be consisted of positive elastic and plastic parts. The latter is defined as the area inside the hysteresis loop at each strain amplitude (cyclic energy) and the former can be calculated from following equation:

$$\Delta E_e^+ = \frac{{\sigma_{max}}^2}{2E} \tag{2}$$

where σ_{max} is the stress at the tensile tip of the hysteresis loop. Through the addition of positive elastic strain energy density, mean stress effect is also taken into account in this model [72]. The energy damage parameter is, then, correlated with fatigue life via an equation analogous to the Coffin-Manson relation [71]:

$$\Delta E = E_e'(2N_f)^B + E_f'(2N_f)^C \tag{3}$$

where ΔE is the total strain energy density. Coefficients and exponents in Eq. (3) are extracted from energy-life curves (Figure 20(a)) and are tabulated in Table 2. The same set of tests as the one used in Figure 19(a) is utilized for parameter extraction in Figure 20(a).

Table 2 Energy-based parameters for JV model.

Fatigue strength coefficient, E_e' (MJ/m^3)	2.995
Fatigue toughness coefficient, E_f' (MJ/m^3)	1710.690
Fatigue strength exponent, B	-0.281
Fatigue toughness exponent, C	-0.975

The plot of total strain energy density versus number of reversals to failure is depicted in Figure 20(b), including the data from literature. As is seen, all the data points can be

consolidated into one single curve. This validates the use of strain energy density for evaluating fatigue damage occurred in AM30 extrusion along different directions, i.e., ED, TD and ND.

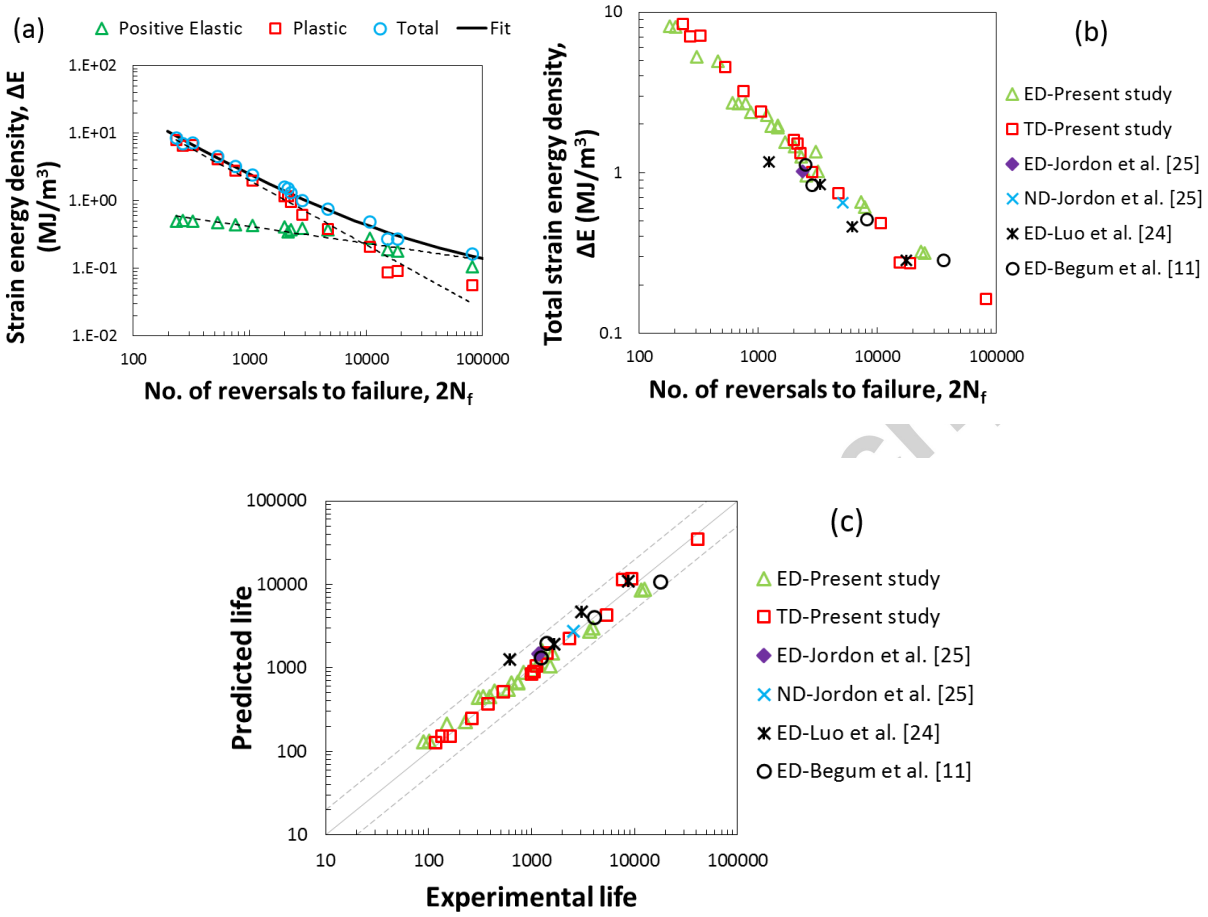

Figure 20 (a) Strain energy-life data used for extracting constants in Eq. (3); (b) JV damage parameter evolution with number of reversals to failure; (c) The correlation of JV-estimated fatigue life with experimental life.

The correlation between predicted life and experimental life in both directions is illustrated in Figure 20(c). All data points fall within the bounds signifying life factor of ±2 (dashed lines). Most of the fatigue life predictions are closely consistent with the observed fatigue life (the data points located on the solid diagonal line). In contrast with the SWT results, the life predictions of the JV model in ED are not scattered, though the maximum stress is

included in this model too. The accuracy of the JV energy model has been also reported to be good in multiaxial fatigue life prediction of AZ31B extrusion [4,65].

5. Conclusions

The uniaxial tension-compression fatigue experiments controlled under fully-reversed condition at various strain amplitudes ranging from 0.3% to 2.3% have been conducted on AM30 Mg alloy extrusion along extrusion (ED) and transverse (TD) directions. Based on the presented results, the following main conclusions can be drawn:

1) The shapes of hysteresis loops in ED and TD are governed by different mechanisms controlling deformation. In both directions, deformation at half-life is dominated by slip when strain amplitude is below 0.5%. Afterwards, twinning/de-twinning becomes predominant deformation mechanism, which is accompanied by asymmetric cyclic response.
2) Extension twinning is believed to happen to a larger extent during compressive reversal along ED compared to TD. This results in higher asymmetry of hysteresis loops in ED.
3) While cyclic hardening is observed along both directions, the stress amplitude and mean stress developed through cyclic loading in ED are higher than those in TD.
4) AM30 extrusion exhibits better fatigue properties when deformed under cyclic loading along TD compared to that in ED, over almost entire strain range tested here. This has been related to the higher fatigue damage induced by means of more extensive twinning as well as higher detrimental mean stress in ED.
5) Fatigue cracks are evidenced to initiate at the specimens' surfaces. Persistent slip bands (PSBs) and twin lamellae interfaces are observed sites of cracking in specimens tested at low and high strain amplitudes, respectively. Cracking/debonding of intermetallic

particles is realized as the common crack initiator in AM30 extrusion under various loading conditions.

6) Jahed-Varvani (JV) energy model gives superior life estimations for AM30 Mg alloy extrusion subjected to cyclic loading, irrespective of loading direction.

Acknowledgement

This study was partially funded by the Natural Sciences and Engineering Research Council (NSERC) under Automotive Partnership of Canada (APC) program. The financial support of the Government of Ontario through Ontario Trillium Scholarship (OTS) program is also acknowledged.

References

[1] H. Friedrich, S. Schumann, Research for a "new age of magnesium" in the automotive industry, J. Mater. Process. Technol. 117 (2001) 276–281.

[2] F. Mokdad, D.L. Chen, Cyclic deformation and anelastic behavior of ZEK100 magnesium alloy: Effect of strain ratio, Mater. Sci. Eng. A. 640 (2015) 243–258.

[3] D. Eliezer, E. Aghion, F. Froes, Magnesium science, technology and applications, Adv. Perform. Mater. 212 (1998) 201–212.

[4] J. Albinmousa, H. Jahed, S. Lambert, Cyclic behaviour of wrought magnesium alloy under multiaxial load, Int. J. Fatigue. 33 (2011) 1127–1139.

[5] J. Albinmousa, H. Jahed, S. Lambert, Cyclic axial and cyclic torsional behaviour of extruded AZ31B magnesium alloy, Int. J. Fatigue. 33 (2011) 1403–1416.

[6] W. Yuan, R.S. Mishra, Grain size and texture effects on deformation behavior of AZ31 magnesium alloy, Mater. Sci. Eng. A. 558 (2012) 716–724.

[7] M.K. Kulekci, Magnesium and its alloys applications in automotive industry, Int. J. Adv. Manuf. Technol. 39 (2007) 851–865.

[8] C. Bettles, M. Gibson, Current wrought magnesium alloys: strengths and weaknesses, JOM. 57 (2005) 46.

[9] E. Doege, K. Dröder, Sheet metal forming of magnesium wrought alloys—formability and process technology, J. Mater. Process. Technol. 115 (2001) 14–19.

[10] S. Begum, D. Chen, S. Xu, A. Luo, Low cycle fatigue properties of an extruded AZ31 magnesium alloy, Int. J. Fatigue. 31 (2009) 726–735.

[11] S. Begum, D.L. Chen, S. Xu, A.A. Luo, Strain-Controlled Low-Cycle Fatigue Properties of a Newly Developed Extruded Magnesium Alloy, Metall. Mater. Trans. A. 39 (2008) 3014–3026.

[12] S.R. Agnew, Ö. Duygulu, Plastic anisotropy and the role of non-basal slip in magnesium alloy AZ31B, Int. J. Plast. 21 (2005) 1161–1193.

[13] Z. Bin Sajuri, Y. Miyashita, Y. Hosokai, Y. Mutoh, Effects of Mn content and texture on fatigue properties of as-cast and extruded AZ61 magnesium alloys, Int. J. Mech. Sci. 48 (2006) 198–209.

[14] S.H. Park, S.-G. Hong, J. Yoon, C.S. Lee, Influence of loading direction on the anisotropic fatigue properties of rolled magnesium alloy, Int. J. Fatigue. 87 (2016) 210–215.

[15] S.H. Park, S.G. Hong, W. Bang, C.S. Lee, Effect of anisotropy on the low-cycle fatigue behavior of rolled AZ31 magnesium alloy, Mater. Sci. Eng. A. 527 (2010) 417–423.

[16] F. Lv, F. Yang, Q.Q. Duan, Y.S. Yang, S.D. Wu, S.X. Li, et al., Fatigue properties of rolled magnesium alloy (AZ31) sheet: Influence of specimen orientation, Int. J. Fatigue. 33 (2011) 672–682.

[17] F. Lv, F. Yang, Q.Q. Duan, T.J. Luo, Y.S. Yang, S.X. Li, et al., Tensile and low-cycle fatigue properties of Mg-2.8% Al-1.1% Zn-0.4% Mn alloy along the transverse and rolling directions, Scr. Mater. 61 (2009) 887–890.

[18] J.B. Jordon, J.B. Gibson, M.F. Horstemeyer, H. El Kadiri, J.C. Baird, A.A. Luo, Effect of twinning, slip, and inclusions on the fatigue anisotropy of extrusion-textured AZ61 magnesium alloy, Mater. Sci. Eng. A. 528 (2011) 6860–6871.

[19] S. Ishihara, Z. Nan, T. Goshima, Effect of microstructure on fatigue behavior of AZ31 magnesium alloy, Mater. Sci. Eng. A. 468-470 (2007) 214–222.

[20] S. Ishihara, S. Taneguchi, H. Shibata, T. Goshima, A. Saiki, Anisotropy of the fatigue behavior of extruded and rolled magnesium alloys, Int. J. Fatigue. 50 (2013) 94–100.

[21] Y.C. Lin, X.-M. Chen, Z.-H. Liu, J. Chen, Investigation of uniaxial low-cycle fatigue failure behavior of hot-rolled AZ91 magnesium alloy, Int. J. Fatigue. 48 (2013) 122–132.

[22] X.M. Chen, Y.C. Lin, J. Chen, Low-cycle fatigue behaviors of hot-rolled AZ91

magnesium alloy under asymmetrical stress-controlled cyclic loadings, J. Alloys Compd. 579 (2013) 540–548.

[23] A.A. Luo, A.K. Sachdev, Development of a New Wrought Magnesium-Aluminum-Manganese Alloy AM30, Metall. Mater. Trans. A. 38 (2007) 1184–1192.

[24] T.J. Luo, Y.S. Yang, W.H. Tong, Q.Q. Duan, X.G. Dong, Fatigue deformation characteristic of as-extruded AM30 magnesium alloy, Mater. Des. 31 (2010) 1617–1621.

[25] J.B. Jordon, H.R. Brown, H. El Kadiri, H.M. Kistler, R.L. Lett, J.C. Baird, et al., Investigation of fatigue anisotropy in an extruded magnesium alloy, Int. J. Fatigue. 51 (2013) 8–14.

[26] C.L. Fan, D.L. Chen, A.A. Luo, Dependence of the distribution of deformation twins on strain amplitudes in an extruded magnesium alloy after cyclic deformation, Mater. Sci. Eng. A. 519 (2009) 38–45.

[27] J. Albinmousa, A. Pascu, H. Jahed, M.F. Horstemeyer, A. Luo, D. Chen, et al., Monotonic and Fatigue Behavior of Magnesium Extrusion Alloy AM30: An International Benchmark Test in the Magnesium Front End Research and Development Project, SAE Tech. Pap. 2010-01-04 (2010) 1–12.

[28] M. Lugo, J.B. Jordon, J. Bernard, M. Horstemeyer, Microstructure-Sensitive Fatigue Modeling of an Extruded AM30 Magnesium Alloy, SAE Tech. Pap. 2013-01-09 (2013).

[29] S. Kleiner, P. Uggowitzer, Mechanical anisotropy of extruded Mg–6% Al–1% Zn alloy, Mater. Sci. Eng. A. 379 (2004) 258–263.

[30] A. Akhtar, E. Teghtsoonian, Solid solution strengthening of magnesium single crystals—ii the effect of solute on the ease of prismatic slip, Acta Metall. 17 (1969) 1351–1356.

[31] C.H. Cáceres, D.M. Rovera, Solid solution strengthening in concentrated Mg-Al alloys, J. Light Met. 1 (2001) 151–156.

[32] Z. Keshavarz, M.R. Barnett, EBSD analysis of deformation modes in Mg-3Al-1Zn, Scr. Mater. 55 (2006) 915–918.

[33] J. Koike, T. Kobayashi, T. Mukai, H. Watanabe, M. Suzuki, K. Maruyama, et al., The activity of non-basal slip systems and dynamic recovery at room temperature in fine-grained AZ31B magnesium alloys, Acta Mater. 51 (2003) 2055–2065.

[34] Y. Xiong, Q. Yu, Y. Jiang, Multiaxial fatigue of extruded AZ31B magnesium alloy, Mater. Sci. Eng. A. 31 (2012) 1–23.

[35] J. Zhang, Q. Yu, Y. Jiang, Q. Li, An experimental study of cyclic deformation of extruded AZ61A magnesium alloy, Int. J. Plast. 27 (2011) 768–787.

[36] L. Wu, A. Jain, D.W. Brown, G.M. Stoica, S.R. Agnew, B. Clausen, et al., Twinning-detwinning behavior during the strain-controlled low-cycle fatigue testing of a wrought magnesium alloy, ZK60A, Acta Mater. 56 (2008) 688–695.

[37] Q. Yu, J. Zhang, Y. Jiang, Fatigue damage development in pure polycrystalline magnesium under cyclic tension-compression loading, Mater. Sci. Eng. A. 528 (2011) 7816–7826.

[38] X.Z. Lin, D.L. Chen, Strain controlled cyclic deformation behavior of an extruded magnesium alloy, Mater. Sci. Eng. A. 496 (2008) 106–113.

[39] S.R. Agnew, D.W. Brown, C.N. Tome, Validating a polycrystal model for the elastoplastic response of magnesium alloy AZ31 using in situ neutron diffraction, Acta Mater. 54 (2006) 4841–4852.

[40] S. Agnew, M. Yoo, C. Tome, Application of texture simulation to understanding mechanical behavior of Mg and solid solution alloys containing Li or Y, Acta Mater. 49 (2001) 4277–4289.

[41] L. Jiang, J.J. Jonas, R.K. Mishra, A.A. Luo, A.K. Sachdev, S. Godet, Twinning and texture development in two Mg alloys subjected to loading along three different strain paths, Acta Mater. 55 (2007) 3899–3910.

[42] L. Jiang, J.J. Jonas, A.A. Luo, A.K. Sachdev, S. Godet, Twinning-induced softening in polycrystalline AM30 Mg alloy at moderate temperatures, Scr. Mater. 54 (2006) 771–775.

[43] M. Niewczas, Lattice correspondence during twinning in hexagonal close-packed crystals, Acta Mater. 58 (2010) 5848–5857.

[44] F. Wang, S.R. Agnew, Dislocation transmutation by tension twinning in magnesium alloy AZ31, Int. J. Plast. 81 (2016) 63–86.

[45] H. El Kadiri, C.D. Barrett, J. Wang, C.N. Tomé, Why are { 10 1^{-} 2 } twins profuse in magnesium?, Acta Mater. 85 (2015) 354–361.

[46] Y. Chino, K. Kimura, M. Hakamada, M. Mabuchi, Mechanical anisotropy due to twinning in an extruded AZ31 Mg alloy, Mater. Sci. Eng. A. 485 (2008) 311–317.

[47] D. Sarker, D.L. Chen, Dependence of compressive deformation on pre-strain and loading direction in an extruded magnesium alloy: Texture, twinning and de-twinning, Mater. Sci.

Eng. A. 596 (2014) 134–144.

[48] D. Sarker, J. Friedman, D.L. Chen, Influence of pre-strain on de-twinning activity in an extruded AM30 magnesium alloy, Mater. Sci. Eng. A. 605 (2014) 73–79.

[49] D. Sarker, D.L. Chen, Texture transformation in an extruded magnesium alloy under pressure, Mater. Sci. Eng. A. 582 (2013) 63–67.

[50] S. Begum, D.L. Chen, S. Xu, A.A. Luo, Effect of strain ratio and strain rate on low cycle fatigue behavior of AZ31 wrought magnesium alloy, Mater. Sci. Eng. A. 517 (2009) 334–343.

[51] X.Y. Lou, M. Li, R.K. Boger, S.R. Agnew, R.H. Wagoner, Hardening evolution of AZ31B Mg sheet, Int. J. Plast. 23 (2007) 44–86.

[52] L. Wu, S.R. Agnew, D.W. Brown, G.M. Stoica, B. Clausen, A. Jain, et al., Internal stress relaxation and load redistribution during the twinning-detwinning-dominated cyclic deformation of a wrought magnesium alloy, ZK60A, Acta Mater. 56 (2008) 3699–3707.

[53] U. Essmann, U. Gösele, H. Mughrabi, A model of extrusions and intrusions in fatigued metals I. Point-defect production and the growth of extrusions, Philos. Mag. A. 44 (1981) 405–426.

[54] H. Mughrabi, R. Wang, K. Differt, U. Essmann, Fatigue Crack Initiation by Cyclic Slip Irreversibilities in High-Cycle Fatigue, Fatigue Mech. Adv. Quant. Meas. Phys. Damage, ASTM STP 811, J. Lankford, D. L. Davidson, W. L. Morris, R. P. Wei, Eds., Am. Soc. Test. Mater. (1983) 5–45.

[55] A. Galiyev, R. Kaibyshev, G. Gottstein, Correlation of plastic deformation and dynamic recrystallization in magnesium alloy ZK60, Acta Mater. 49 (2001) 1199–1207.

[56] K. Gall, G. Biallas, H.J. Maier, P. Gullett, M.F. Horstemeyer, D.L. McDowell, In-situ observations of low-cycle fatigue damage in cast AM60B magnesium in an environmental scanning electron microscope, Metall. Mater. Trans. A. 35 (2004) 321–331.

[57] K. Gall, G. Biallas, H.J. Maier, P. Gullett, M.F. Horstemeyer, D.L. McDowell, et al., In-situ observations of high cycle fatigue mechanisms in cast AM60B magnesium in vacuum and water vapor environments, Int. J. Fatigue. 26 (2004) 59–70.

[58] G. Murugan, K. Raghukandan, U.T.S. Pillai, B.C. Pai, K. Mahadevan, High cyclic fatigue characteristics of gravity cast AZ91 magnesium alloy subjected to transverse load, Mater. Des. 30 (2009) 2636–2641.

[59] F. Wang, J. Dong, M. Feng, J. Sun, W. Ding, Y. Jiang, A study of fatigue damage development in extruded Mg-Gd-Y magnesium alloy, Mater. Sci. Eng. A. 589 (2014) 209–216.

[60] Y. Xiong, Y. Jiang, Fatigue of ZK60 magnesium alloy under uniaxial loading, Int. J. Fatigue. 64 (2014) 74–83.

[61] D.L. Chen, A.R. Emami, A.A. Luo, Cyclic deformation of extruded AM30 magnesium alloy in the transverse direction, J. Phys. Conf. Ser. 240 (2010).

[62] J.D. Bernard, J.B. Jordon, M.F. Horstemeyer, H.E. Kadiri, J. Baird, D. Lamb, et al., Structure-property relations of cyclic damage in a wrought magnesium alloy, Scr. Mater. 63 (2010) 751–756.

[63] W. Song, H.J. Martin, A. Hicks, D. Seely, C.A. Walton, W.B. Lawrimore, et al., Corrosion behaviour of extruded AM30 magnesium alloy under salt-spray and immersion environments, Corros. Sci. 78 (2014) 353–368.

[64] Y. Xiong, Q. Yu, Y. Jiang, An experimental study of cyclic plastic deformation of extruded ZK60 magnesium alloy under uniaxial loading at room temperature, Int. J. Plast. 53 (2014) 107–124.

[65] J. Albinmousa, H. Jahed, Multiaxial effects on LCF behaviour and fatigue failure of AZ31B magnesium extrusion, Int. J. Fatigue. 67 (2014) 103–116.

[66] E. Kalatehmollaei, H. Mahmoudi-Asl, H. Jahed, An asymmetric elastic-plastic analysis of the load-controlled rotating bending test and its application in the fatigue life estimation of wrought magnesium AZ31B, Int. J. Fatigue. 64 (2014) 33–41.

[67] H. Jahed, J. Albinmousa, Multiaxial behaviour of wrought magnesium alloys - A review and suitability of energy-based fatigue life model, Theor. Appl. Fract. Mech. 73 (2014) 97–108.

[68] Y.C. Lin, Z.H. Liu, X.M. Chen, J. Chen, Stress-based fatigue life prediction models for AZ31B magnesium alloy under single-step and multi-step asymmetric stress-controlled cyclic loadings, Comput. Mater. Sci. 73 (2013) 128–138.

[69] D.F. Socie, Multiaxial Fatigue Damage Models, J. Eng. Mater. Technol. 109 (1987) 293–298.

[70] R.N. Smith, P. Watson, T.H. Topper, A Stress Strain Function for the Fatigue of Metals, J. Mater. JMLSA. 5 (1970) 767–778.

[71] H. Jahed, A. Varvani-Farahani, Upper and lower fatigue life limits model using energy-based fatigue properties, Int. J. Fatigue. 28 (2006) 467–473.

[72] K. Golos, F. Ellyin, A Total Strain Energy Density Theory for Cumulative Fatigue Damage, J. Press. Vessel Technol. 110 (1988) 36–41.